Journal of Statistical Physics, Vol. 128, Nos. 1/2, July 2007 (© 2007)
DOI: 10.1007/s10955-006-9202-z

A Mesoscopic Simulation Approach for Modeling Intracellular Reactions

Ramon Grima[1] and Santiago Schnell[1]

Received January 31, 2006; accepted August 28, 2006
Published Online October 4, 2006

Reactions in the intracellular medium occur in a highly organized and heterogenous environment rendering invalid modeling approaches based on the law of mass action or its stochastic counter-part. This has led to the recent development of a variety of stochastic microscopic approaches based on lattice-gas automata or Brownian dynamics. The main disadvantage of these methods is that they are computationally intensive. We propose a mesoscopic method which permits the efficient simulation of reactions occurring in the complex geometries typical of intracellular environments. This approach is used to model the transport of a substrate through a pore in a semi-permeable membrane, in which its Michaelis–Menten enzyme is embedded. We find that the temporal evolution of the substrate is a sensitive function of the spatial heterogeneity of the environment. The spatial organization and heterogeneities of the intracellular medium seem to be playing an important role in the regulation of biochemical reactions.

KEY WORDS: macromolecular crowding, modeling intracellular reactions, biological processes in organized media, mesoscopic simulation

1. INTRODUCTION

Biochemical reactions are the basis of cellular functions. They occur in an intracellular environment which abounds with organelles and macromolecules. The high macromolecular content of the cytoplasm, known as macromolecular crowding,[23,25,31] implies that between 5% and 40% of the total intracellular volume is physically occupied by these molecules. This is much larger than the density typically found *in vitro* conditions.[67] Also it is known that many of the proteins and transmembrane receptors which carry and process messages inside a living cell are associated with compact clusters of molecules attached to cell membranes

[1] Indiana University School of Informatics and Biocomplexity Institute, 1900 East Tenth Street, Bloomington, IN 47406, USA; e-mail: rgrime, schnell@indiana.edu.

or the cytoskeleton.[7] The small scale compartmentalization induced by both crowding and internal cellular architecture imply that the *in vivo* environment, unlike the *in vitro* one, is highly heterogeneous.

In recent years computational modeling has become a tool to investigate various phenomena in the natural sciences. Traditionally the modeling of chemical reactions has been achieved either by means of differential equations based on the law of mass action or through the use of its stochastic counter-part.[72] Unfortunately, these two approaches have been demonstrated both theoretically[37,38,72] and experimentally[47,48] to be invalid for describing reactions occurring in heterogenous environments, particularly in dimensionally-restricted conditions.

Notwithstanding the vast evidence to the contrary, the majority of intracellular modeling studies assume that the classical law of mass action is valid (for recent examples see Refs. 11, 27, 52, 64). This obviously simplifies the problem but nevertheless is physico-chemically incorrect. In the past few years two approaches have been developed to counteract this problem, namely that of realistically simulating and investigating reactions occurring in a spatially extended heterogeneous environment: (i) the Lattice-Gas (LG) or Monte Carlo method[6,67] and (ii) *Smoldyn*, a Brownian dynamics simulator.[2]

Lattice-gas automata were originally devised as a method for the simulation of fluid flows.[22,26,32] They have since proved to provide a simple, phenomenological and easily implementable method of investigating the macroscopic dynamics of chemical reaction kinetics. This is achieved by averaging over noisy data obtained from the stochastic simulation of a large number of point molecules moving and interacting on a spatial lattice according to a well defined set of rules. LG simulations have a long history of being applied to reactions occurring in homogeneous media.[34–36,73]It is however only recently that they have been applied to study the kinetics of biochemical reactions in an *in vivo* biological setting. A few examples of such studies are: signaling in T Lymphoctes,[18] signal transduction in *E. coli* chemotaxis[43] and enzyme and bimolecular reactions occurring on two dimensional membranes.[29,67] LG simulations provide a simple but powerful framework for building models of intracellular transport and signaling, though to date this has only been used in a few instances. The main problem with this type of modeling is that we are usually not interested in the reaction kinetics on the scale of a single molecule or of a few molecules but rather on the scale of a typical organelle. To obtain such information from LG simulations, a substantial amount of noise averaging is needed, leading to long simulation times. This problem is fundamentally similar to that of coarse graining in LG simulations of fluid flow in complex geometries.[26]

The advantage of the Brownian dynamics simulator, *Smoldyn*, over LG is that it does not have an artificial spatial lattice, thus eliminating possible lattice effects.[29] It however shares the same disadvantage of LG, namely that it provides

Table I. Typical spatial scales inside a cell[10]

	Size range
Animal cells	10 μm–100 μm
Nucleus	$\sim$5 μm
Mitochondrion	$\sim$2 μm
Ribosomes	$\sim$30 nm
Proteins	4 nm–10 nm
Small molecules	0.5 nm–1 nm

single molecule detail. An added disadvantage is that molecular crowding and organelles have to be simulated via three dimensional shapes constructed by patching together several flat surfaces. This enhances the difficulty of simulating reaction kinetics in realistic intracellular geometries.

Our aim in this article is to develop a modeling environment which enables the buildup of a reasonably realistic picture of intracellular signaling in large parts of the cell, with a resolution of say 1/100th of the size of a typical cell. Current microscopic methods are impractical; coarse graining of the reaction dynamics means that simulations take a very long time, putting a dire limit on what is realistically possible to investigate.[62,65,72] In Sec. 2 we develop a lattice mesoscopic (LM) technique which surmounts the problems of the current approaches. This approach is put to the test in Sec. 3 and we conclude with a discussion in Sec. 4.

2. A MESOSCOPIC MODEL

The most important feature of our novel approach is that it should describe the reactive kinetics on a mesoscopic scale, in a manner which is consistent with the relevant physics and chemistry at this scale. We arbitrarily choose this scale to be much larger than that of individual molecules but smaller than that of an organelle. Such a scale separation is indeed possible since as shown in Table I the size of a typical organelle is about three orders of magnitude larger than that of small molecules.

We start by overlaying a square grid over the portion of intracellular space of interest. For simplicity, we will model reactions in a two dimensional environment though the extension to three dimensions is straightforward. Let the grid resolution be Δx; the N elements of the grid are each identified by an integer number j. Each element of the grid has associated with it two types of number densities: $[\rho_R^i]_j$ and $[\rho_U]_j$, where $[\rho_R^i]_j$ is the number density of the ith reactive chemical species in element j and $[\rho_U]_j$ is the number density of unreactive microscopic objects in element j. Unreactive objects can, for example, represent inert cytoplasmic macromolecular agents or microscopic portions of intracellular structures such as

organelles. We shall assume that reactive molecules are mobile whereas unreactive objects are static. This assumption can be easily relaxed though generally speaking macromolecules and organelles are relatively static compared to the more mobile reactant molecules. The total density in element j is the sum of the number densities of all reactive and unreactive objects in the element and is denoted by $[\rho_T]_j$. Inside each element of the grid, two physical processes are modeled: (i) the diffusive influx and outflux from the four neighboring elements, (ii) the interaction of reactive molecular species inside the element. We shall assume that these two processes can be decoupled from each other. Then the diffusive dynamics can be described by a master equation with some transition rates $W_{k\to j}$ and the reactive dynamics can be described by some function F of the molecular number densities:

$$\partial_t\left[\rho_R^i\right]_j = \sum_k \left[W_{k\to j}\left[\rho_R^i\right]_k - W_{j\to k}\left[\rho_R^i\right]_j\right] + F\left(\left[\rho_R^i\right]_j, \left[\rho_R^m\right]_j\right), \qquad (1)$$

where the sum over k is a sum over the four nearest element neighbors of element j and m denotes all reactive species which through interaction with other species either produce or destroy species i. Of course, if we ignore the inter-molecular and hydrodynamic forces between all chemical species and the physical confinement due to the cell's internal architecture, then the reactions occur in a well-mixed environment; in such a case the above equation would be reduced to a conventional reaction-diffusion type of equation with transition rates $W_{k\to j} = D/\Delta x^2$ (the constant D is a diffusion coefficient for the molecules) and reaction terms directly proportional to the product of reactant concentrations (follows from the law of mass action).

However, as previously mentioned intracellular environments are replete with unreactive objects, ranging in size from microscopic macromolecular agents to large organelles such as mitochondria. Hence it is clear that the diffusion of reactant molecules of say type i, from one element a to a neighboring one b, cannot be pure diffusion. Rather in computing the diffusive flux, one has to take into account the number densities of both reactive and unreactive species in elements a and b. We could model this in a phenomenological manner by defining heuristic rules which qualitatively reproduce density-dependent diffusion. Unfortunately, this approach would produce a model defined in terms of parameters which are not experimentally measurable, thus limiting the quantitative predictions of the model. Instead we choose to derive the physically correct diffusive reaction kinetics by coarse-graining the relevant microscopic Langevin equations, thereby obtaining the correct form of the transition rate $W_{k\to j}$. This is left for Sec. 2.1. The reaction of the various molecular species inside an element is also affected by the population of unreactive objects inside the element meaning that we need a new functional form for the reactive terms F. This is treated in Sec. 2.2.

2.1. Derivation of the Diffusive Influx/Outflux Equations

Let us derive the physically correct form of the diffusive currents between neighboring elements of the grid. For the moment we ignore the elements of the grid. We only consider reactive and unreactive molecules in continuous space. Consider the interaction of N_A molecules of type A, N_B molecules of type B and N_O molecules of type O. A and B are reactive species while O is an unreactive species. The motion of a single molecule of type A is determined by an equation of motion of the Langevin type:

$$\dot{\mathbf{x}}_{A,n}(t) = \xi_{A,n}(t) + \sum_{m=1,m\neq n}^{N_A} \nabla V(\mathbf{x}_{A,n} - \mathbf{x}_{A,m}) + \sum_{m=1}^{N_B} \nabla V(\mathbf{x}_{A,n} - \mathbf{x}_{B,m}) + \sum_{m=1}^{N_O} \nabla V(\mathbf{x}_{A,n} - \mathbf{x}_{O,m}), \tag{2}$$

where $\mathbf{x}_{A,n}$ is the center of mass of the nth molecule of type A. The stochastic variable $\xi_{A,n}$ is white noise defined by $\langle \xi_{A,n}(t) \rangle = 0$ and the correlation function $\langle \xi_{A,n}(t)\xi_{A,m}(t') \rangle = 2D\delta_{n,m}\delta(t - t')$, where D is the diffusion coefficient of the molecules. The angular brackets $\langle\rangle$ denote the ensemble average. The intermolecular interaction is mediated by the potential function V. Thus the above equation describes the diffusion and intermolecular interaction of molecules of type A with all other molecules. Note that it does not describe the reaction kinetics since this is taken care of separately in the next section.

The correlation function above implies that we are assuming that molecular movement in the absence of intermolecular forces mediated by the potential V, can be well described by a Wiener process, which is a model of Brownian motion.[24] This model is an idealized one and thus the simplest; the Ornstein-Uhlenbeck process is a more realistic model of Brownian motion but we do not treat it further in this article. By assuming Brownian motion, we are implicitly assuming that the reactant molecules of interest are much larger than the background fluid molecules, whose thermal motion is responsible for the reactant molecules' haphazard Brownian movement. The fluid molecules are not modeled in our approach. The effect that they have on the reactant molecules' motion is purely through the diffusion coefficient D.

We emphasize that D is the diffusion coefficient of isolated reactive or unreactive molecules i.e. in the absence of any interaction (through a force field) with other similar molecules. Note that our formulation implicitly ignores hydrodynamic interactions (see the Discussion section for more on this). Thus although it is clear that the effective diffusion coefficient of reactive or unreactive molecules has to be a function of the spatio-temporal configuration of other molecules, this fact cannot be introduced *a priori* through D. Rather it has to naturally come out

when we take into account the intermolecular forces between molecules. We shall calculate the effective diffusion coefficient later in this section.

Since our proposed model is at a mesoscopic scale we are interested in number densities not individual molecules. To this end we now derive an equation of motion for the molecule probability density function using Eq. (2). Let $P_{A,n}(\mathbf{x}, t)$ be the probability that the nth molecule of type A is at position $\mathbf{x}$ at time t. Then it can be shown[50] that Eq. (2) is exactly equivalent to the following equation of motion for the molecular probability density function:

$$\partial_t P_{A,n}(\mathbf{x}, t) = D\nabla^2 P_{A,n}(\mathbf{x}, t) + \nabla \cdot \int d^d x' \, [\nabla V(|\mathbf{x} - \mathbf{x}'|)] \sum_{m \neq n} P_{A,n|A,m}(\mathbf{x}, t; \mathbf{x}', t)$$
$$+ \nabla \cdot \int d^d x' \, [\nabla V(|\mathbf{x} - \mathbf{x}'|)] \sum_{m} P_{A,n|B,m}(\mathbf{x}, t; \mathbf{x}', t)$$
$$+ \nabla \cdot \int d^d x' \, [\nabla V(|\mathbf{x} - \mathbf{x}'|)] \sum_{m} P_{A,n|O,m}(\mathbf{x}, t; \mathbf{x}', t), \tag{3}$$

where $P_{A,n|O,m}(\mathbf{x}, t; \mathbf{x}', t)$ is the probability that at time t, the nth molecule of type A is at position $\mathbf{x}$ while the mth molecule of type O is at position $\mathbf{x}'$. We refer to this as the two molecule joint probability density function. Note that an implicit assumption used in deriving this equation is that the diffusion coefficient of all reactant molecules of type A is exactly the same. We also assumed that all molecules interact through the same type of potential. This restrictive assumption is not generally required to derive the above equation, the only requirement being that molecules of one type interact with molecules of another type through the same potential. For example it is possible that molecules of type A react with each other through a potential V and with molecules of type B and O through a different potential V_0. In such a case the potential V in the third and fourth terms on the right hand side of Eq. (3) would be replaced by V_0. For the sake of simplicity, throughout the rest of our treatment we will assume that all molecules interact through the same potential V.

Having obtained an equation of motion for the single molecule probability density function, we now want to use this to derive an equation for the temporal evolution of the number density. Let R denote a general molecule of any type. Applying the mean field approximation $P_{A,n|R,m} = P_{A,n} P_{R,m}$ (ignoring statistical correlations between molecules) to Eq. (3) and summing the resulting equation over the index n we find an equation for the number density of molecules of type A, $\rho_A(\mathbf{x}, t)$:

$$\partial_t \rho_A = D\nabla^2 \rho_A + \nabla \cdot \rho_A \nabla \int d^d x' \left[V(|\mathbf{x} - \mathbf{x}'|) \rho(\mathbf{x}', t) \right], \tag{4}$$

where $\rho(\mathbf{x}, t) = \rho_A(\mathbf{x}, t) + \rho_B(\mathbf{x}, t) + \rho_O(\mathbf{x}, t)$ i.e. ρ is the total number of molecules of any kind at position $\mathbf{x}$ at time t. In a similar manner one can derive equations for molecules of species B. The validity and implications of using the mean-field approximation is discussed at the end of this subsection.

Eq. (4) is continuous in space and time. By discretizing it we obtain the relevant dynamics in our lattice mesoscopic model. This discretization can be performed in many ways; we choose the MED representation[28] which guarantees that the discretized equation has the form of a Master equation.[24,63] Let the velocity potential function be defined as:

$$\phi(\mathbf{x}, t) = \int d^d x' V(|\mathbf{x} - \mathbf{x}'|)\rho(\mathbf{x}', t). \tag{5}$$

Then the MED discretized form of Eq. (4) is:

$$\partial_t \left[\rho_R^1\right]_j = \sum_k \left[W_{k\to j}\left[\rho_R^1\right]_k - W_{j\to k}\left[\rho_R^1\right]_j\right], \tag{6}$$

where $[\rho_R^1]_j$ is the number density of molecules of species A in element j. Note that the notation $[\rho_R^i]_j$ was introduced in the previous section; here we have chosen $i = 1$ to denote species A. The sum is over the nearest element neighbors of element j. $W_{j\to k}$ is the transition rate for molecules of type A to move from element j to element k. This is given by:

$$W_{k\to j} = \frac{D}{\Delta x^2}\, e^{-(\Phi_j - \Phi_k)/2D}, \tag{7}$$

where Δx is the lattice spacing of our mesoscopic approach and Φ_j is the discretized form of the velocity potential:

$$\Phi_j = \sum_{k'} V(|(j - k')\Delta x|)[\rho_T]_{k'}. \tag{8}$$

In this expression, the sum over k' is a sum of all the grid elements covering the intracellular space of interest. The potential function V is sampled by the discretized velocity potential at integer multiples of the grid size Δx. This means that details of the potential function over distances smaller than the grid size are irrelevant. Since our model by design is mesoscopic, the grid size is much larger than that of individual molecules implying that any discretized intermolecular potential function can be well approximated by a delta-function $V(|\mathbf{x} - \mathbf{x}'|) = U_0\delta(\mathbf{x} - \mathbf{x}')$. Thus the discretized velocity potential function reduces to the simple form:

$$\Phi_j = U_0\,[\rho_T]_j, \tag{9}$$

where U_0 is a constant measuring the strength of repulsion between molecules. Hence the transition rate for molecules to move between two neighboring grid

elements, j and k, is given by:

$$W_{j\to k} = \frac{D}{\Delta x^2}\, e^{-U_0([\rho_T]_k - [\rho_T]_j)/2D}. \tag{10}$$

This completely specifies the diffusive dynamics part of the general mesoscopic equation Eq. (1). We note that the physical meaning of this transition rate is that on a coarse enough spatial scale, the combined effect of diffusion and intermolecular potential-mediated interactions is equivalent to a spatially and directionally-dependent diffusion.

Now we briefly discuss the assumptions implicit in using the above approach for modeling the diffusive motion of reactant molecules in a heterogeneous environment. The crucial approximation at the heart of our derivation is the mean-field approximation. One may ask what is the need of such an approximation and what does it imply about our method's validity and general applicability. Eq. (3) is an exact probabilistic description of the Langevin model given by Eq. (2). The single molecule probability density function $P_{A,n}(\mathbf{x}, t)$ can be computed if one knows the two molecule joint probability density function $P_{A,n|O,m}(\mathbf{x}, t; \mathbf{x}', t)$. One can also derive equations for the two molecule joint probability density function, thus finding that it depends on the three molecule joint probability density function. Hence the corresponding probabilistic description of the Langevin equation consists of a hierarchy of a large number of coupled equations which generally cannot be solved. One can use these equations together with perturbation theory in momentum space to derive expressions for averaged quantities, for example the time dependence of the spatial variance of the molecules, but it is not possible to derive an effective macroscopic equation in terms of the number density of molecules, which is our aim. The problem clearly stems from the spatial correlations between molecules. By ignoring these correlations (applying the mean-field approximation) one can get an equation for the temporal evolution of the molecular number density.

Now such an approximation is well-known to be generally valid in higher dimensions and for large numbers of interacting particles. An environment characterized by a very high spatial heterogeneity is one in which the effective dimensionality and the number of interacting molecules is small. The latter follows from the fact that if there is a large number of static obstacles then mobile reactant molecules have a tendency of becoming trapped in small areas of space, thus isolating them from interaction with the rest of the reactant molecules. Hence our approach should be fine for low to moderate heterogeneous spatial regions but will breakdown for highly heterogeneous parts of the intracellular space of interest. In particular in highly heterogeneous regions, the molecular movement in reality should be described by anomalous diffusion[51] not Fickian diffusion thus implying that in these regions our approach will probably over-estimate the movement of molecules from one grid element to neighboring ones. The validity

of the mean-field approximation is also dependent on the mobility of intracellular obstacles; if the obstacles are mobile, then the approximation holds better than for the case of static obstacles.

2.2. Non-Classical Reaction Kinetics

In the previous section, we have considered the effect of unreactive objects on the diffusive flux in and out of a given element. The reaction of the various molecular species inside an element is also affected by the population of unreactive objects inside the element. This applies only to bimolecular reactions which are diffusion-limited but does not apply to monomolecular reactions. We shall assume throughout this section that there are only two reactive species A and B and an unreactive non-mobile species O. Furthermore we assume that the two reactant species interact through an elementary bimolecular reaction of the type $A + B \rightarrow$ ø. We choose this example for illustrative purposes, however all the results we shall find apply equally well to more complex reaction mechanisms with any number of reacting species. The specific aim of this section is to find an appropriate form for the reaction function F in the general mesoscopic equation Eq. (1).

The simplest mathematical form for the function F describing the reactive dynamics in element j is given by $F = -k[\rho_R^1]_j[\rho_R^2]_j$. Here k is the reaction constant characterizing the reaction $A + B \rightarrow$ ø, $[\rho_R^1]_j$ is the number density of species A in element j and $[\rho_R^2]_j$ is the number density of species B in element j. This form for F is clearly not suitable for our purposes since it is based on the law of mass action, which is generally valid for reactions occurring in homogeneous and high dimensional environments.

In recent years, reaction kinetics in heterogenous conditions has been approximated mostly by two methods, fractal kinetics and the power-law approximation, both of which are a modification of the law of mass action. In the fractal kinetics approach,[38] the rate constant k is replaced by a rate coefficient $k(t)$ with a time dependence whose asymptotic form is proportional to t^{-h}, where $0 < h < 1$. Unfortunately this approach is not compatible with a mesoscopic model of intracellular kinetics. This method is only valid for closed systems, whereas each element of our grid is an open system (molecules can freely enter and leave). A second possible approach would be the power-law approximation of Savageau.[66,67] In this approach the reaction orders are not restricted to the integer values given by the law of mass action but rather they can take fractional values dependent on the fracton dimension of the environment. It is valid for both open and closed systems and thus it is generally compatible with a mesoscopic description. The main problem in adopting this approach is that it has been proven correct only for elementary reactions[30] under a restricted set of initial conditions. A second problem is that the power-law approximation is a phenomenological approach and as such there is

no clear connection with the relevant physics. Given these limitations we choose not to employ it.

Instead we opt for a simpler method derived from a first-principles physics consideration of the reaction kinetics. We first assume that both reactive and unreactive species are distributed randomly inside the element. Then the encounter rate of reactive molecules of type A and B has to be proportional to the sum of their respective self-diffusion coefficients:

$$\text{encounter rate} = k\left[\rho_R^1\right]_j\left[\rho_R^2\right]_j, \tag{11}$$

$$k \propto (D_1 + D_2), \tag{12}$$

where k is the rate coefficient. Thus to compute the rate coefficient we need expressions for the self-diffusion coefficient. The self-diffusion coefficient is the transport coefficient characterizing the dynamical time evolution of the single particle density. It depends on the inter-particle forces mediated by a potential and also on hydrodynamic interactions. Specific analytic forms of the self-diffusion coefficient are only known for a few inter-particle potential functions, usually in the limit of small concentration.[9] Thus although the exact form of the intermolecular potential will not have much effect on the diffusive currents between neighboring elements of our grid (as we showed in the previous section), it is a significant factor in determining the reaction kinetics. Our ensuing discussion of the appropriate form of the self-diffusion coefficient will be in the context of the shape of the chemical species under consideration. The reactive chemical species inside cells can be proteins or other smaller types of molecules, for example simple sugars. However the inert macromolecules which crowd the cytoplasm are frequently proteins. There are three general cases which ought to be considered:

(i) both reactive and unreactive molecules are spherical particles,
(ii) reactants are spherical particles while the unreactive molecules have a non-spherical shape,
(iii) both reactive and unreactive molecules have non-spherical configurations.

Proteins are either globular (spherical) or fibrous (non-spherical) polymers. Enzymes are frequently globular proteins while fibrous proteins tend to have a structural, inert function. It is thus unlikely that both reactant and unreactant molecules are spherical; the chances are that at least one of them is non-spherical. The self-diffusion coefficient is a function of the geometrical configuration of the interacting molecules. We shall briefly consider the above three cases.

The case in which both reactive and unreactive particles have spherical configurations is analogous to the self-diffusion of spheres in suspension. This is a well studied problem, particularly for the case of uncharged spheres whose motion is coupled via the fluid.[3,4,20] An analysis which takes into account the many-body hydrodynamics interactions[4] shows that the self-diffusion coefficient for a dilute

suspension is given by:

$$D \propto 1 - 1.73\psi + 0.88\psi^2 + O(\psi^3), \tag{13}$$

where ψ is the excluded volume fraction of space. Similar results are known for charged spheres (with and without hydrodynamic interactions), though in this case the coefficients in the series expansion above are not constants; rather they are functions of the parameters characterizing the interaction potential.[9]

Next the case where the reactant is spherical and the unreactive molecules are not. Assuming hard sphere interactions, the reduction in reactant diffusivity due to a background inert polymer network has been shown by many studies (see for example, Refs. 33, 51, 70) to follow a stretched exponential law in the volume fraction. This law breaks down for high fractions of excluded volume, marked by the onset of anomalous diffusion.[51] The non-spherical polymer networks used in these studies consisted of worm-like chains and various porous cage-like structures.

If both reactive and unreactive molecules do not have spherical configurations (e.g. polymer chains) then the analysis becomes considerably more complicated. As recently remarked by Merriam *et al.* (page 1663, Ref. 46) "the theoretical elucidation of the nature of polymer dynamics remains a substantial challenge for theoretical statistical mechanics." The underlying reason for this difficulty is that many forces contribute to polymer-polymer interactions, including: (i) topological restrictions due to chain crossing constraints, (ii) solvent-mediated hydrodynamics interactions, (iii) excluded volume effects, (iv) interactions leading to long-lived inter-chain associations.[46] There exist a large number of models to explain polymer dynamics. These theories can be broadly divided into two main categories: (i) those that deal with hydrodynamic interactions and which give little importance to configurational properties of the polymer[1,12,55] (ii) those which neglect hydrodynamic interactions and instead focus on the geometry and structural properties of the polymeric systems[53,60,61]. A number of hydrodynamic theories based on scaling[12,40,56] and more recently using renormalization group analysis[57] show that the diffusion coefficient of a polymer in a background polymer solution (of the same type or of a different type) is given by the simple relation:

$$D \propto \exp(-gc^{\beta}), \tag{14}$$

where c is the polymer concentration and g and β are a scaling pre-factor and exponent respectively. This stretched exponential law is essentially the same as the one for hard spherical particles in a medium consisting of non-spherical ones, which we discussed in the previous paragraph. On the other hand, theories focusing on the configurational properties of the polymers give different results, in particular a different dependence of the diffusion coefficient on the polymer concentration c. These models are largely based on the work of Edwards[16,17] and de

Gennes.[13,14] There are at least two distinctive regimes predicted by these models: (i) dilute solutions, in which the polymer molecules move practically independent of each other and the diffusion coefficient is a constant (ii) semi-dilute and concentrated solutions (polymer melts) in which self-diffusion occurs by a process called reptation. In the latter process, polymer chains move predominantly parallel to their own backbones. It is predicted[8,13] that the concentration dependence of the self-diffusion coefficient in this regime is:

$$D \propto c^{-\gamma}, \tag{15}$$

where $\gamma \in (1.75, 3)$. Despite these predictions, a systematic re-examination of the experimental literature on polymer self-diffusion[58,59] finds that the self-diffusion coefficient of polymers in solution is described by a stretched exponential law in c over very wide ranges of c. This law is the same as that obtained from hydrodynamic theories [Eq. (14)]. It leads to the conclusion that probably reptation is not generally important for polymers in solution. However, it may well be important for highly concentrated solutions (polymer melts) in which the dynamics are dominated by polymer-polymer friction. The general consensus to date appears to be that the diffusion of large molecules in polymer solutions is well described by the stretched exponential law.[54] However it must be emphasized that "no one model of diffusion can as yet successfully treat solute diffusion in polymer solutions over a wide range of solute sizes and polymer concentrations" (page 6031, Ref. 54).

For our model we use the stretched exponential law given by Eq. (14) since this is the form which fits well many experimental data and which has a strong theoretical underpinning. Other advantages are: (i) it describes well two of the three cases of possible geometrical configurations of reactive and unreactive molecules, and (ii) it is empirically correct over wide ranges of the excluded volume fraction of space, irrespective of the actual physical mechanisms at work.

The exact physical significance of the constants g and β in the stretched exponential law differs from one model to another. It is empirically[58] found that β is about one but g varies over about five orders of magnitude. The constant g depends on the type of interaction potential and thus on the relative sizes and shapes of all molecules, both the reacting ones and also those which form the inert background. We replace the concentration c in Eq. (14) by ψ, the excluded volume fraction of space, since they are proportional. We also set $\beta = 1$. Thus we shall use the expression $D \propto e^{-g\psi}$ for the self-diffusion coefficient of reactant molecules. This expression was first suggested to study intracellular crowding by Minton.[47] Note that for small values of the excluded volume the above expression reduces to the one describing the self-diffusion coefficient of spheres in suspension Eq. (13). We use this equation to calculate the rate coefficient of a reactant species in each element of the mesoscopic grid. Based on previous arguments, the reaction rate

of a species is proportional to the self-diffusion coefficient. Thus the form of the reactive function F in element j in the general mesoscopic equation Eq. (1) is given by:

$$F = -k_{12} \exp(-g\psi_j)\left[\rho_R^1\right]_j \left[\rho_R^2\right]_j, \tag{16}$$

where k_{12} is the rate constant in the limit of infinite dilution and ψ_j is the the fractional occupancy (excluded volume) in element j of the mesoscopic grid, which is given by:

$$\psi_j = \sum_i \left[\rho_R^i\right]_j v_i + \left[\rho_U\right]_j v_u. \tag{17}$$

The parameter v_i is the volume of a single molecule of reactive species i and v_u is the volume of a single unreactive molecule. The form of F given by Eq. (16) is specifically for the reaction $A + B \rightarrow \text{ø}$. Many complex reaction mechanisms can be decomposed into elementary monomolecular and bimolecular reaction steps. As previously mentioned the monomolecular steps are not diffusion-limited and so can be modeled as usual; the bimolecular steps can be modeled via terms of the form given by Eq. (16).

We conclude this subsection by noting that g is a measure of crowding effects on the reaction kinetics. Setting $g = 0$ implies that excluded volume effects due to crowding are insignificant—this is tantamount to assuming that the law of mass action holds. In many cases, reactions will involve charged species; in such cases g is expected to be a function of the details of the long-range interaction potential. Results for macroions interacting through a Debye-Huckel potential form[9] suggest that g is proportional to the strength of repulsion (for small excluded volume fractions) implying a possible similar relationship between g and U_0 (the latter parameter was introduced in the previous section). For the purposes of this paper, it shall be assumed that the latter two constants are independent, since we do not enforce a specific type of inter-molecular potential. Note that as for the case of diffusive dynamics, our method for modeling the reactive dynamics fails for high obstacle densities, since the onset of anomalous diffusion precludes the use of a self-diffusion coefficient on which our method is based.

2.3. Summary of Method

Let us now put together the diffusive and reaction kinetics derived in previous sections to obtain the lattice mesoscopic method. The intracellular space of interest is subdivided into a certain number of square elements with side Δx. This scale is chosen much larger than that of a single molecule but smaller than that of a typical organelle. Each element j has associated with it two types of number densities $[\rho_R^i]_j$ and $[\rho_U]_j$, where $[\rho_R^i]_j$ is the number density of the ith reactive chemical species in element j and $[\rho_U]_j$ is the number density of unreactive microscopic

objects in the same element. We assume the unreactive species to be static and the reactive species to be mobile. The total number density of all species in element j is given by $[\rho_T]_j = \sum_i [\rho_R^i]_j + [\rho_U]_j$.

The mesoscopic equation describing the movement and reaction of the reactive molecular species of type i in element j is then given by:

$$\partial_t \left[\rho_R^i\right]_j = \sum_k \left[W_{k\to j}\left[\rho_R^i\right]_k - W_{j\to k}\left[\rho_R^i\right]_j\right] - \sum_m k_{im} e^{-g\psi_j}\left[\rho_R^i\right]_j\left[\rho_R^m\right]_j + \sum_{u,v} k_{uv} e^{-g\psi_j}\left[\rho_R^u\right]_j\left[\rho_R^v\right]_j, \tag{18}$$

where

$$\psi_j = \sum_i \left[\rho_R^i\right]_j v_i + [\rho_U]_j v_u, \tag{19}$$

$$W_{k\to j} = \frac{D}{\Delta x^2} e^{-U_0([\rho_T]_j - [\rho_T]_k)/2D}. \tag{20}$$

In Eq. (18), the sum over k is a sum over the nearest element neighbors of element j. The sum over m is a sum over all molecular species in element j which react with species i to form some other product molecule. The sum over u and v is a sum over all molecular species u and v in element j which react to produce species i. All reactions are assumed to be bimolecular. Note that monomolecular reactions, such as the irreversible decay of a species into two other types, are not diffusion-limited and thus would be modeled by an equation in which the rate coefficient is a constant (this implies that $g = 0$). The method's general use is illustrated in the next section where we model intracellular enzyme-mediated reactions composed of both monomolecular and bimolecular reaction steps.

The numerical scheme at the heart of our method, Eq. (18), gives meaningful results only for values of the time step Δt and of the space step Δx guaranteeing numerical stability of the method. A stability analysis can be found in Appendix A. The temporal derivative on the left hand side of Eq. (18) can be discretized by a first-order accurate Euler approximation. Let the maximum spatial gradient in the total number density of molecules in the intracellular space of interest be q and let k_{im} be the rate constant characteristic of the bimolecular reaction between the ith and mth reactive species. Then we find that stability is achieved if the time step Δt satisfies the condition:

$$\Delta t \le \min\left[\frac{1}{\max k_{im}}, \frac{\Delta x^2}{2D\cosh q U_0 \Delta x/2D}\right]. \tag{21}$$

3. CHEMICAL DIFFUSION THROUGH THE PLASMA MEMBRANE: A CASE STUDY

The structural organization of the cytoplasm and assembly of proteins into larger structures may confer advantages. For example, they can promote metabolic channeling, resistance of hydrolytic enzymes, and the reduction of proteins or other active molecules for cell functioning.[69] In this section, we model the transport of a substrate through a pore in a semi-permeable membrane, in which its Michaelis–Menten enzyme is embedded. A similar set up has been used to study experimentally the kinetics data of membrane-bounded enzymes and transport systems.[68] The purpose of simulating this system is to test the LM technique, particularly the ability to simulate two key processes which are common to all reactions in intracellular environments. These processes are: (a) the diffusion of chemicals through media having a certain amount of permeability; (b) the reaction kinetics in spatial environments characterized by macromolecular crowding and non-trivial geometry.

We simulate the diffusion of a substrate S through a pore in a portion of the semi-permeable cellular plasma membrane. The physical setup is illustrated in Fig. 1. Enzyme is embedded in the membrane (green area) at two different locations (red areas). The substrate and enzyme molecules react following the Michaelis–Menten mechanism to yield product molecules P. Our initial condition consists of a uniform concentration of substrate molecules placed on the left side of the membrane (grey area). In our simulation, we are interested in understanding the temporal evolution of the substrate concentration field.

3.1. Implementation

We model our reacting environment as a 100×100 square grid with the origin being located at the lower left corner of the grid. Molecules are initially distributed as follows:

(i) 10000 molecules of substrate S are randomly placed on nodes of the grid with position (i, j) such that $1 \leq i \leq 40$ and $1 \leq j \leq 100$.
(ii) 500 molecules of enzyme E are randomly placed on nodes of the grid with position $40 \leq i \leq 50$ and $30 \leq j \leq 40$. Another 500 molecules of enzyme E are randomly placed on nodes of the grid with position $50 \leq i \leq 60$ and $60 \leq j \leq 70$.
(iii) 10000 unreactive molecules are randomly placed on nodes of the grid with position $40 \leq i \leq 60$ and $1 \leq j \leq 40$. Another 10000 unreactive molecules are randomly placed on nodes of the grid with position $40 \leq i \leq 60$ and $60 \leq j \leq 100$. These inert molecules represent the membrane.

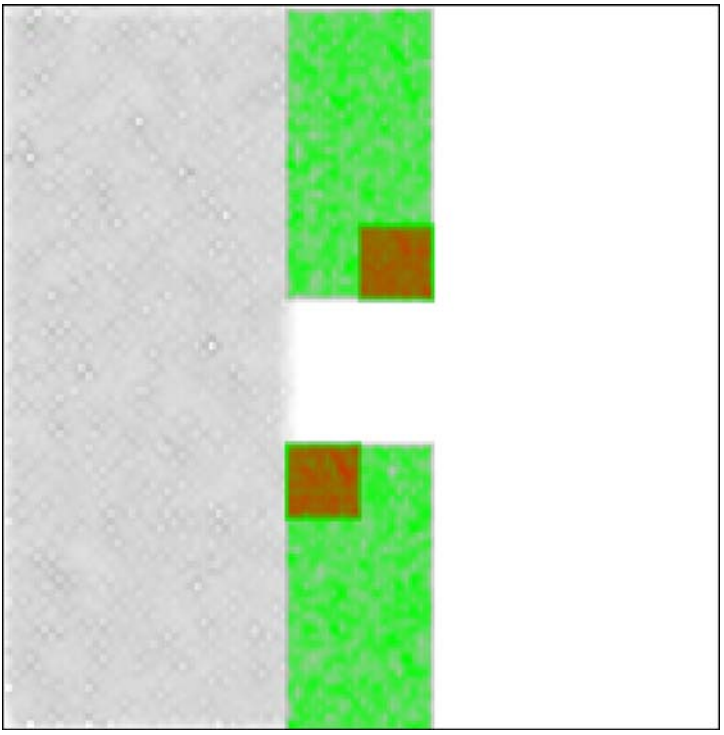

Fig. 1. Setup of our model system. The cellular membrane (green area) has enzyme at two different locations (red areas). Initially the substrate is uniformly concentrated on the left side of the membrane (grey area). Color online.

The number density of molecules of a certain type at each grid node is defined as the total number of molecules of that type located at that node. To be precise, in obtaining the density one needs to scale by the area of each element but we ignore this since it does not qualitatively change the results. Note that the time evolution is completely in terms of the density; unlike simulations with LG and *Smoldyn*, molecules are not moved individually. Let $[\rho_R^i]_j$ be the number density of the ith reactive molecular species in element j. In our case $i \in 1, 2, 3, 4$, where $i = 1$ is the substrate, $i = 2$ is the enzyme, $i = 3$ is the enzyme-substrate complex, and $i = 4$ is the product. There is only one unreactive species, the membrane molecules, whose number density in element j is denoted by $[\rho_U]_j$. The total number density of all species in element j is denoted by $[\rho_T]_j$. Then the equations defining the temporal evolution of the reactive density at an element j, according to the LM model prescription Eq. (18)

are:

$$\partial_t\left[\rho_R^1\right]_j = \sum_k \left[W_{k\to j}\left[\rho_R^1\right]_k - W_{j\to k}\left[\rho_R^1\right]_j\right] - k_{12}e^{-g\psi_j}\left[\rho_R^1\right]_j\left[\rho_R^2\right]_j + k_{21}\left[\rho_R^3\right]_j, \tag{22}$$

$$\partial_t\left[\rho_R^2\right]_j = -k_{12}e^{-g\psi_j}\left[\rho_R^1\right]_j\left[\rho_R^2\right]_j + (k_{21}+k_3)\left[\rho_R^3\right]_j, \tag{23}$$

$$\partial_t\left[\rho_R^3\right]_j = k_{12}e^{-g\psi_j}\left[\rho_R^1\right]_j\left[\rho_R^2\right]_j - (k_{21}+k_3)\left[\rho_R^3\right]_j, \tag{24}$$

$$\partial_t\left[\rho_R^4\right]_j = \sum_k \left[W_{k\to j}\left[\rho_R^4\right]_k - W_{j\to k}\left[\rho_R^4\right]_j\right] + k_3\left[\rho_R^3\right]_j. \tag{25}$$

The sum over k is the sum over the four nearest neighbors of element j. k_{12} is the rate of reaction of substrate and enzyme, k_{21} is the rate of decay of the complex into the enzyme and the substrate, and k_3 is the rate of decay of the complex into enzyme and product. Note that only the substrate and product diffuse. The rest are immobile. Please also note that only the diffusion-limited steps of the reaction have an exponential factor multiplied by the rate constant. Note that there are no equations for the unreactive molecule number density since this does not evolve in time. In our simulations $\Delta x = 10^{-1}$ and $\Delta t = 10^{-3}$. The values of the rate constants are: $k_{12} = 10$, $k_{21} = 0.1$ and $k_3 = 5$. The diffusion coefficient D is set to unity and the molecular repulsion constant $U_0 = 0.1$. For simplicity the molecular volume of all species, reactive and unreactive, is chosen to be equal; as can be verified from the definition of the fractional occupancy Eq. (17), this implies $\psi_j \propto [\rho_T]_j$ in our model equations. The boundary conditions are fixed: the value of all molecular number densities is zero on the boundary at all times.

One may ask if the chosen parameters are appropriate for the biological case modeled. Because of the large variety of chemicals which diffuse through the membrane and of the even larger number of possible enzyme-mediated reactions, there are no typical rate constants and diffusion coefficients that we may use. Our rate constants are chosen so that the enzyme reaction proceeds very quickly in the forward direction; this ensures quick production of the product which is typical of many biochemical reactions.[21]

3.2. Results

The temporal evolution of the density field for the substrate species is computed after 5000 time steps and after 50000 time steps (note that the substrate concentration field in the latter case does not represent the steady state of the system). This is computed for two cases: (i) $g = 0$, that is, assuming that crowding effects are unimportant (Fig. 2) (ii) $g = 1$ which implies the contrary (Fig. 3). Note that the evolution of the density field is markedly different for the two cases. There

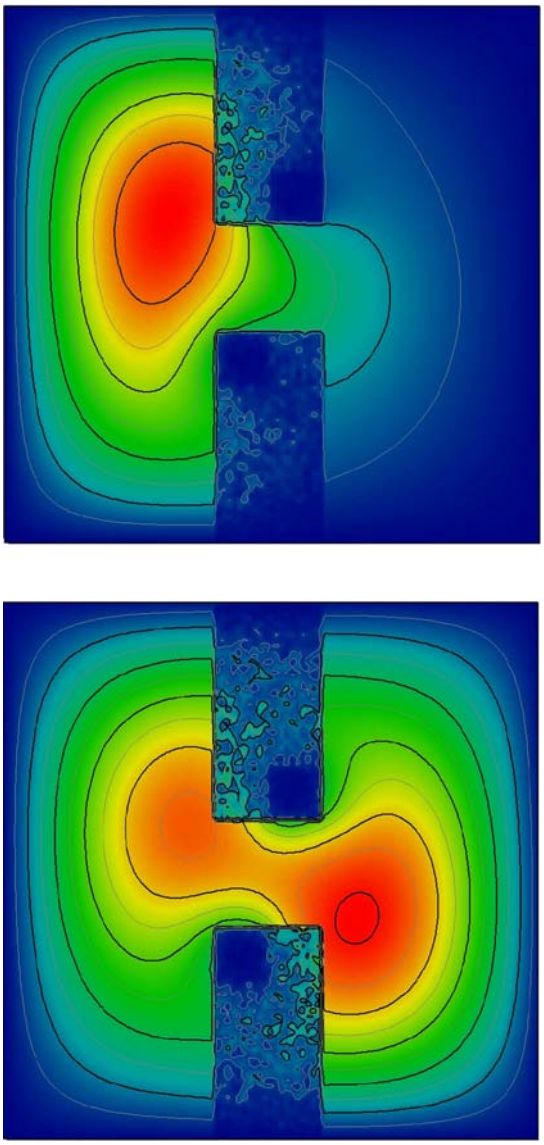

Fig. 2. Contour plot of the number density of the substrate field for $g = 0$ at (a) t = 5 $\times 10^3$ time steps (b) t = 5 $\times 10^4$ time steps. The relative magnitude of the number density in a region is indicated by the color of the region, ranging from blue for low densities to red for the highest densities. Note that the same color in (a) and (b) does NOT mean that the magnitude of the concentration is the same in both regions of the two separate figures. The color gradient for each individual figure is calculated according to the maximum and minimum density in that particular figure. Color online.

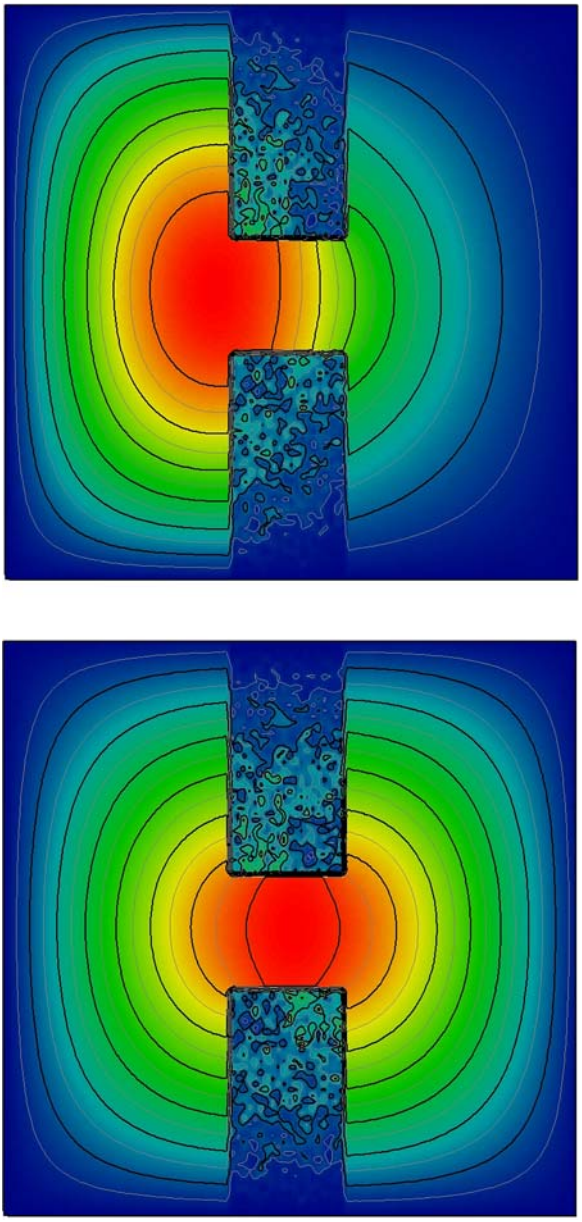

Fig. 3. Contour plot of the number density of the substrate field for $g = 1$ at (a) $t = 5 \times 10^3$ time steps (b) $t = 5 \times 10^4$ time steps. The color gradient is calculated as for Fig. 2. Color online.

are three notable differences between low and high crowding effects which are evident at sufficiently long times: (i) the direction of substrate transport through the pore (ii) the absolute magnitude of the substrate density maximum (iii) the location of the substrate density maximum.

When crowding is negligible, $g = 0$, there is a high rate of enzyme-catalyzed reactions in spatial regions close to those parts of the membrane which contain the localized enzyme. This explains the asymmetry of the density at the entrance of the pore at $t = 5000$ time steps and the low density in the middle of the pore at $t = 50000$ time steps. When crowding is significant, $g = 1$, the rate of enzyme-catalyzed reactions near the enzyme embedded regions is significantly reduced when compared to that for $g = 0$. Thus there is no asymmetry in the density field at early or later times. The direction of substrate transport and its spatial distribution are directly related to the symmetry/asymmetry considerations just discussed.

The second difference is directly related to the rate of reaction: $g = 0$ implies a higher rate of reaction and thus smaller values of the maximum number density than for the case $g = 1$.

The third requires some explanation. For $g = 0$, the high rate of reaction at the center of the pore causes a larger concentration gradient than for the case $g = 1$. Thus the substrate diffuses quicker through the pore for the case $g = 0$ than for the other case. This time lag between the two cases is clearly shown by plotting the substrate number density at the center of the pore, as a function of time (Fig. 4).

Note that in practice, both values of g may be applicable in different parts of the cell. The magnitude of g depends on the relative sizes and shapes of the reactant species and the inert space-filling species,[47] and in particular on the interaction potential. If U_0 is assumed to be proportional to g (as we hypothesized in Sec. 2.2) then the same qualitative results as above are obtained. However in this case, the differences between low and highly crowded conditions are further exacerbated – this is since the substrate diffusive flux into the enzyme embedded regions is inversely proportional to U_0 (see Eq. (10)).

Our simulations clearly show that crowding considerations are an important (though very often neglected) determining factor in the time evolution of intracellular biochemical reactions. We have also illustrated the power of our novel modeling approach: we simulated a complex reacting system with diffusion of chemicals through semi-permeable membranes and reaction kinetics in complex geometries.

4. DISCUSSION

In this article we have introduced a new modeling framework for investigating the effect of macromolecular crowding and cellular architecture on the

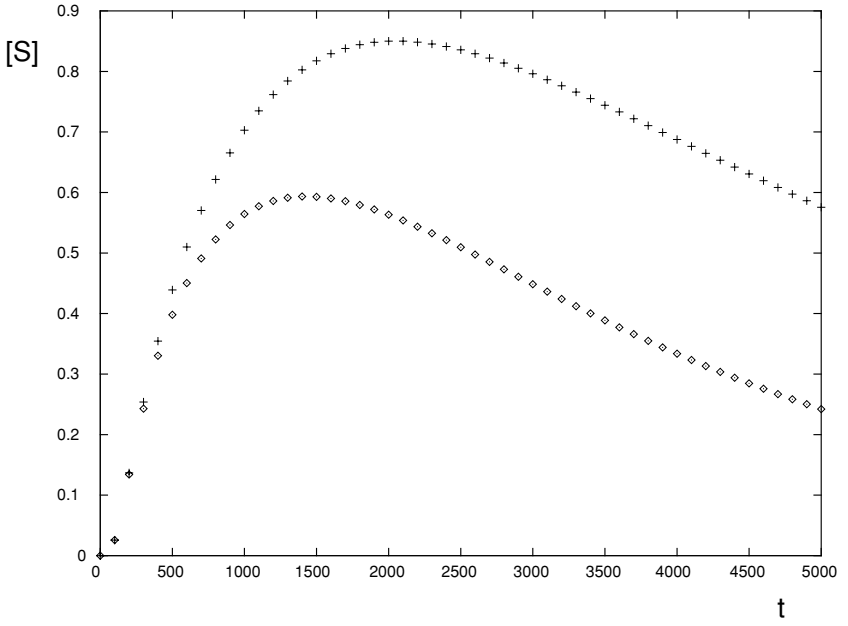

Fig. 4. Plot of the substrate density $[S]$ in the center of the membrane pore as a function of time (t is the number of time steps) for $g = 0$ (diamond points) and $g = 1$ (cross points).

temporal evolution of intracellular biochemical reactions. The main advantages of the LM technique over current techniques is that it models the mesoscopic reaction kinetics rather than the microscopic reaction kinetics. It also enables to potentially build realistic models of a whole cell with a resolution of the order of a typical organelle. Indeed the advantages of the LM technique over the current microscopic approaches are analogous to those of the Lattice Boltzmann method over the lattice-gas automata models of fluid flow.[26]

We note that our approach is based on an over-damped form of a multi-particle Langevin equation Eq. (2) for the reactant and obstacle molecules. Of course this is only approximative; a physically more realistic treatment would require starting from the Hamiltonian equations of motion.[15,41,45] The conditions under which such equations reduce to a set of coupled over-damped Langevin equations and the conditions under which the Stokes law formula can be used for the friction (as we have implicitly used) have been extensively discussed by Oppenheim and collaborators.[15,45,71] The form of the Langevin equation which we used as our starting point can only be justified, if the hydrodynamic forces between the Brownian particles are insignificant compared to those due to intermolecular potentials over the relevant temporal and spatial scales. A more general

formulation including hydrodynamic interactions requires that the diffusion coefficient D in our Langevin equations is not a scalar constant (as we have assumed) but rather a tensor whose components are a function of the inter-particle distances.[19,49] The specific forms of this tensor depend on the shapes of the particles and the hydrodynamical boundary conditions at their surfaces, information which is generally not available.[49] The conditions in which hydrodynamical interactions may be relevant to macromolecular crowding have been discussed by Bernado *et al.*[5]

One of the most important discoveries from the past decade of cell signalling research is that the physical location of proteins plays a central role in intracellular reaction kinetics.[7,39] In recent years, it has also become clear that macromolecular crowding and diffusion impose biophysical constraints[44] which influence the evolution of cell signaling pathways. In agreement with these observations, we show that the structural organization of the reaction medium is important in enzyme catalysis (see, Figs. 2–3).

To date, both experiment and theory show that crowded conditions inside cells strongly favor associations between macromolecules, often increasing the binding affinity of molecules.[48] Interestingly, we find two new effects of the macromolecular crowding on the reaction kinetics. The presence of crowding agents affects the direction and rate of substrate transport through a pore in the plasma membrane. At the same time, crowding increases the substrate concentration, and therefore its availability in the reacting systems. We note that our simulations are based on a stretched exponential form for the rate coefficient of reactant molecules inside the cells. This description is fine when one or more of the interacting molecules has a non-spherical configuration but may overestimate crowding when both reactant and inert molecules are spherical. This may occur, for example, if both types of molecules are globular proteins. Thus in specific regions of the cell where such conditions may occur, it may be difficult to observe some of the predictions we have made.

Our simulations show that biophysical constraints resulting from cellular organization and macromolecular crowding affect the diffusive transport of substrates. It is likely that the intracellular spatial organization and biophysical constraints of macromolecular crowding have played a role in the evolution of cell signaling pathways.

APPENDIX A: STABILITY ANALYSIS

In this section we perform a stability analysis of the explicit numerical scheme at the heart of our mesoscopic approach. The aim is to find a suitable time step for efficiently and accurately simulating an intracellular scenario of interest. The numerical scheme has a reactive part and a diffusive-advective part.

The reactive dynamics are characterized by timescales $\tau_{im} = 1/k_{im}$, where k_{im} is the rate constant for the bimolecular reaction between the ith and mth reactive species. Thus the time step has to be chosen much smaller than the smallest timescale, which is that given by the largest rate constant:

$$\Delta t = \min \tau_{im} = 1/\max k_{im}. \tag{26}$$

The time step required to guarantee the stability of the diffusive-advective part of the numerical scheme can be determined by a conventional Von Neumann analysis.[42] The diffusive-advective dynamics of reactive species A in element j are described by the equation:

$$\partial_t \left[\rho_R^i\right]_j = \frac{D}{\Delta x^2} \sum_k e^{-U_0([\rho_T]_j - [\rho_T]_k)/2D} \left[\rho_R^i\right]_k - e^{-U_0([\rho_T]_k - [\rho_T]_j)/2D} \left[\rho_R^i\right]_j. \tag{27}$$

We shall consider the one dimensional form of the equation; later we will generalize the analysis to higher dimensions. Then Eq. (27) can be written as:

$$\begin{aligned}\left[\rho_R^i\right]_j(t+\Delta t) = \left[\rho_R^i\right]_j(t) + \frac{D\Delta t}{\Delta x^2}\Big(& e^{-U_0([\rho_T]_j - [\rho_T]_{j+1})/2D} \left[\rho_R^i\right]_{j+1}(t) \\ & + e^{-U_0([\rho_T]_j - [\rho_T]_{j-1})/2D}\left[\rho_R^i\right]_{j-1}(t) - e^{-U_0([\rho_T]_{j+1} - [\rho_T]_j)/2D} \left[\rho_R^i\right]_j(t) \\ & - e^{-U_0([\rho_T]_{j-1} - [\rho_T]_j)/2D} \left[\rho_R^i\right]_j(t)\Big),\end{aligned} \tag{28}$$

where we discretized the temporal derivative by an Euler forward approximation, which is first-order accurate in time. Now we proceed with the stability analysis. The principle behind it is that the amplitude of any Fourier mode of the system must decay with time. Note that for a purely advective system the amplitude would have to stay constant but generally diffusion is also present and thus the amplitude must decay with time. Consider the time evolution of a single Fourier mode of wave-number k:

$$[\rho_R^i]_j(t) = A(t)\exp(ikj\Delta x). \tag{29}$$

Note that the i inside the exponent does not refer to the ith reactive species but is the square root of -1. Substituting the above equation in Eq. (28) and simplifying, we obtain:

$$\theta = \frac{A(t+\Delta t)}{A(t)} = 1 - \frac{\alpha D\Delta t}{\Delta x^2}(1-\cos k\Delta x) - i\frac{\alpha\beta D\Delta t}{\Delta x^2}\sin k\Delta x, \tag{30}$$

where

$$\alpha = e^{-U_0([\rho_T]_j - [\rho_T]_{j+1})/2D} + e^{-U_0([\rho_T]_j - [\rho_T]_{j-1})/2D}, \tag{31}$$

$$\beta = \frac{e^{-U_0([\rho_T]_j - [\rho_T]_{j-1})/2D} - e^{-U_0([\rho_T]_j - [\rho_T]_{j+1})/2D}}{e^{-U_0([\rho_T]_j - [\rho_T]_{j+1})/2D} + e^{-U_0([\rho_T]_j - [\rho_T]_{j-1})/2D}}. \tag{32}$$

For stability, the amplitude must decrease with time; thus we require that the modulus of θ must be less than unity. It can be shown that this condition is met if:

$$\frac{\alpha D \Delta t}{\Delta x^2} \leq 1, \tag{33}$$

$$\beta \leq 1. \tag{34}$$

The second condition is always fulfilled, by definition of β above. Hence only the first condition needs to be met to guarantee stability. The minimum value of the time step Δt is determined by the maximum value of α, which can be estimated in the following manner. Let the maximum spatial gradient in the total number density of molecules in the intracellular space of interest be q. Furthermore assume that the grid is fine enough so that this gradient is present over at least two elements of our grid i.e $[\rho_T]_{j+1} - [\rho_T]_j = [\rho_T]_j - [\rho_T]_{j-1} = q\Delta x$. Then the stability condition can be written as:

$$\Delta t \leq \frac{\Delta x^2}{2D \cosh q U_0 \Delta x / 2D}. \tag{35}$$

Hence to ensure stability and accuracy for both the reactive and the diffusion-advective parts of the numerical scheme at the heart of our mesoscopic method, the time step must be chosen to satisfy the two constraints: Eq. (26) and Eq. (35). Our derivation for the second constraint was in one dimension; the more general result in arbitrary number of dimensions, gives the same equation with a small modification: the right hand side is divided by the dimensionality.

ACKNOWLEDGMENTS

We are very grateful to Michel Thellier (L'université de Rouen, France) for his critical reading of the manuscript. We thank two anonymous referees for their helpful comments. The authors gratefully acknowledge support by a grant from the Faculty Research Support Program from the OVPR, Indiana University (Bloomington Campus).

REFERENCES

1. A. R. Altenberger and M. Tirrell, *J. Chem. Phys.* **80**: 2208 (1984).
2. S. S. Andrews and D. Bray *Phys. Biol.* **1**: 137 (2004).
3. G. K. Batchelor *J. Fluid Mech.* **74**: 1 (1976).
4. C. W. J. Beenakker and P. Mazur *Physica A***120**: 388 (1983).
5. P. Bernado, J. G. de la Torre and M. Pons *J. Mol. Recognit.* **17**: 397 (2004).
6. H. Berry *Biophys. J.* **83**: 1891 (2002).

7. D. Bray *Annu. Rev. Biophys. Biomol. Struct.* **27**: 59 (1998).
8. F. Brochard and P.-G. DeGennes, *Macromolecules* **10**: 1157 (1977).
9. D. F. Calef and J. M. Deutch, *Ann. Rev. Phys. Chem.* **34**: 493 (1983).
10. N. A. Campbell, *Biology* (The Benjamin/Cummings Publishing Company, California, 1996).
11. B. Cheng, R. L. Fournier, and P. A. Relue, *Biotechnol. Bioeng.* **70**: 467 (2000).
12. R. I. Cukier *Macromolecules* **17**: 252 (1984).
13. P.-G. DeGennes *Macromolecules* **9**: 594 (1976).
14. P.-G. DeGennes *Scaling Concepts in Polymer Physics* (Cornell University Press, Ithaca, 1979).
15. J. M. Deutch and I. Oppenheim *J. Chem. Phys.* **54**: 3547 (1971).
16. M. Doi and S. F. Edwards *The Theory of Polymer Dynamics* (Oxford University Press, Oxford, 1986).
17. S. F. Edwards, *J. Phys. A* **8**: 1670 (1975).
18. J. L. Eide and A. K. Chakraborty *J. Phys. Chem. B*. **110**: 2318 (2006).
19. D. L. Ermak and J. A. McCammon *J. Chem. Phys.* **69**: 1352 (1978).
20. B. U. Felderhof *J. Phys. A* **11**: 929 (1978).
21. A. R. Fersht *Structure and Mechanism in Protein Science: A Guide to Enzyme Catalysis and Protein Folding*, (Freeman, New York, 1999).
22. U. Frisch, B. Hasslacher and Y. Pomeau *Phys. Rev. Letts.* **56**: 1505 (1986).
23. A. B. Fulton *Cell* **30**: 345 (1982).
24. C. W. Gardiner *Handbook of Stochastic Methods*, 2nd edition (Springer, Berlin, 1995).
25. N. D. Gershon, K. R. Porter and B. L. Trus *Proc. Natl. Acad. Sci USA* **82**: 5030 (1985).
26. D. A. Wolf-Gladrow *Lattice-Gas Cellular Automata and Lattice-Boltzmann Models: An Introduction* (Springer, Berlin, 2000).
27. A. Goldbeter *Biochemical oscillations and cellular rhythms* (Cambridge University Press, 1996).
28. R. Grima and T. J. Newman *Phys. Rev. E* **70**: 036703 (2004).
29. R. Grima and S. Schnell *Biophysical Chemistry*. DOI:10.1016/j.bpc.2006.04.019.
30. R. Grima and S. Schnell *Chem. Phys. Chem.* **7**: 1422 (2006).
31. D. Hall and A. P. Minton *BBA-Proteins Proteomics* **1649**: 127 (2003).
32. J. Hardy, Y. Pomeau and O. D. Pazzis *J. Math. Phys.* **14**: 1746 (1973).
33. L. Johansson and J.-E Lofroth, *J. Chem. Phys.* **98**: 7471 (1993).
34. R. Kapral, A. Lawniczak and P. Masiar *Phys. Rev. Lett.* **66**: 2539 (1991).
35. R. Kapral, A. Lawniczak and P. Masiar, *J. Chem. Phys.* **96**: 2762 (1992).
36. L. B. Kier, C.-K. Cheng and P. G. Seybold *Reviews in Computational Chemistry* Vol. 17 (John Wiley and Sons Inc., New York, 2001), pp. 205–254.
37. R. Kopelman *J. Stat. Phys.* **42**: 185 (1986).
38. R. Kopelman *Science* **241**: 1620 (1988).
39. H. Kuthan *Prog. Biophys. Mol. Biol.* **75**: 1 (2001).
40. D. Langevin and F. Rondelez, *Polymer* **19**: 875 (1978).
41. J. L. Lebowitz and E. Rubin *Phys. Rev.* **131**: 2381 (1963).
42. R. J. LeVeque *Numerical Methods for Conservation Laws* (Birkhauser, Basel, 1990).
43. K. Lipkow, S. S. Andrews and D. Bray *J. Bact.* **187**: 45 (2005).
44. K. Luby-Phelps *Int. Rev. Cytol.* **192**: 189 (2000).
45. P. Mazur and I. Oppenheim *Physica* **50**: 241 (1970).
46. S. C. Merriam and G. D. J. Phillies *J. Poly. Sci. Part B* **42**: 1663 (2004).
47. A. P. Minton *Biopolymers* **20**: 2093 (1981).
48. A. P. Minton *J. Biol. Chem.* **276**: 10577 (2001).
49. T. J. Murphy and J. L. Aguirre *J. Chem. Phys.* **57**: 2098 (1972).
50. T. J. Newman and R. Grima *Phys. Rev. E.* **70**: 051916 (2004).
51. P. A. Netz and T. Dorfmuller *J. Chem. Phys.* **107**: 9221 (1997).
52. B. Novak, Z. Pataki, A. Ciliberto and J. J. Tyson *Chaos* **11**: 277 (2001).

53. A. G. Ogston, B. N. Preston and J. D. Wells *Proc. R. Soc. London, Ser. A* **333**: 297 (1973).
54. J. M. Petit, B. Roux, X. X. Zhu and P. M. Macdonald *Macromolecules* **29**: 6031 (1996).
55. G. D. J. Phillies *J. Phys. Chem.* **93**: 5029 (1989).
56. G. D. J. Phillies *Macromolecules* **20**: 558 (1987).
57. G. D. J. Phillies *Macromolecules* **31**: 2317 (1998).
58. G. D. J. Phillies *Macromolecules* **19**: 2367 (1986).
59. G. D. J. Phillies *J. Phys. Chem.* **96**: 10061 (1992).
60. C. G. Phillips and K. M. Jansons *Macromolecules* **23**: 1717 (1990).
61. C. G. Phillips *J. Chem. Phys.* **95**: 4593 (1991).
62. D. C. Rapaport *The Art of Molecular Dynamics Simulation*, 2nd edition (Cambridge University Press, 2004).
63. H. Risken *The Fokker-Planck Equation* (Springer, Berlin, 1989).
64. J. M. Rohwer, P. W. Postma, B. N. Kholodenko, and H. V. Westerhoff *Proc. Natl. Acad. Sci. U.S.A.* **95**: 10547 (1998).
65. J. Rottler and A. C. Maggs *Phys. Rev. Lett.* **93**: 170201 (2004).
66. M. A. Savageau *J. Theor. Biol.* **176**: 115 (1995).
67. S. Schnell and T. E. Turner *Prog. Biophys. Mol. Biol.* **85**: 235 (2004).
68. M. Thellier, J.-C. Vincent, S. Alexandre, J.-P. Lassalles, B. Deschrevel, V. Norris and C. Ripoll *C. R. Biologies* **326**: 149 (2003).
69. M. Thellier, G. Legent, V. Norris, C. Baron and C. Ripoll *C. R. Biologies* **327**: 1017 (2004).
70. M. Tokita, T. Miyoshi, K. Takegoshi and K. Hikichi *Phys. Rev. E* **53**: 1823 (1996).
71. M. Tokuyama and I. Oppenheim *Physica A* **94**: 501 (1978).
72. T. E. Turner, S. Schnell and K. Burrage *Comp. Biol. Chem.* **28**: 165 (2004).
73. V. Zehnle and G. Searby *J. Phys. Paris* **50**: 1083 (1989)